Received: 25 January 2023 | Revised: 29 April 2023 | Accepted: 29 May 2023

DOI: 10.1002/suco.202300062

ARTICLE

fib CEB-FIP WILEY

Crack monitoring on concrete structures: Comparison of various distributed fiber optic sensors with digital image correlation method

Max Herbers[1] | Bertram Richter[1] | Daniel Gebauer[1] | Martin Classen[2] | Steffen Marx[1]

[1]Technische Universität Dresden, Institute of Concrete Structures, Dresden, Germany

[2]RWTH Aachen, Institute of Structural Concrete, Aachen, Germany

Correspondence
Max Herbers, Technische Universität Dresden, Institute of Concrete Structures, 01062 Dresden, Germany.
Email: max.herbers@tu-dresden.de

Funding information
Ministry for Digital and Transport, Germany

Abstract

The quality of strain measurements using distributed fiber optic sensors (DFOS) depends largely on the bond between the host material and the optical fiber. Experimental investigations were carried out to test the suitability of five different DFOS types for crack monitoring. The DFOS were subsequently bonded to two 4 m long reinforced concrete (RC) beams, so that the influence of the application technique could be evaluated. DFOS measurements were verified by digital image correlation (DIC) and electrical strain gauges (SGs). For the different DFOS types, clear differences in the measured strain curves and determined crack widths were observed. The focus was on two robust DFOS, which can be deployed on construction sites. Compared to the layered sensing cable, a monolithic DFOS showed a clear strain distribution with pronounced strain peaks even for closely spaced cracks. The crack widths obtained by integrating the strain curves showed high agreement with DIC measurements.

KEYWORDS

crack monitoring, crack width calculation, DFOS, DFOS type, distributed fiber optic sensing, existing concrete bridges, installation technique

1 | INTRODUCTION

1.1 | Challenges of aging infrastructure

Infrastructure in Germany, as in many other European countries, is aging. The majority of bridges were built during the 1960s and 1970s[1] and are therefore gradually reaching the end of their service life. Thus, maintaining existing structures will be crucial in the upcoming decades to ensure mobility and reduce the use of resources through demolition and reconstruction. To allow existing structures to be used for a prolonged

Abbreviations: ACR, acrylate; BOTDR, BRILLOUIN optical time domain reflectometry; c-OFDR, coherent optical frequency domain reflectometry; DFOS, distributed fiber optic sensor; DIC, digital image correlation; DSS, distributed strain sensing; DTS, distributed temperature sensing; ES, EpsilonSensor; NYL, polyamid/nylon; ODiSI, optical distributed sensor interrogator 9; ORM, ORMOCER®; PA, polyamid; PE, polyester; POL, polyimid; RC, reinforced concrete; SG, strain gauge; SHM, structural health monitoring; SLS, serviceability limit state; TS, tension stiffening.

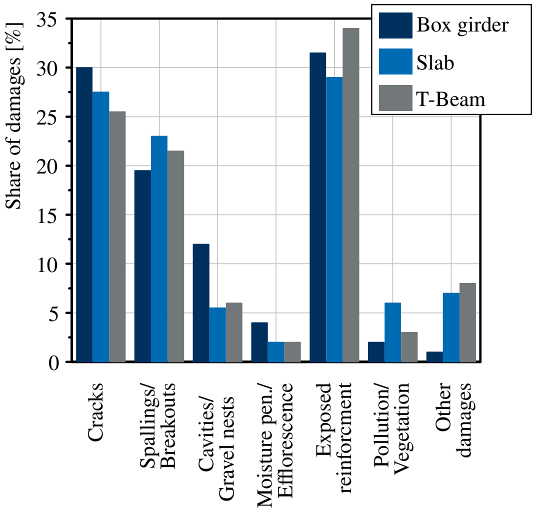

FIGURE 1 Distribution of damages of superstructures of solid bridges (basis: 2991 damages on box girders, 4763 damages on slabs, 6745 damages on T/beams).[13]

period of time while maintaining the same level of safety, the concept of the digital twin[2–4] gains popularity in the construction industry. In digital twins, structural health monitoring (SHM)[5–8] serves as the most important link between the real object and its virtual representation, allowing structures to be monitored in near real time and also a prediction of their condition can be made.[9,10] Measurement errors[11] and influences from aging measurement systems[12] can negatively affect the quality of the monitoring data and must therefore be corrected automatically.

Figure 1 illustrates that a large part of the damages to superstructures of concrete bridges can be attributed to cracking. In addition, spalling and the exposure of steel reinforcement are further damage patterns, promoted by the formation of cracks. With the current periodic structural inspections, the crack pattern is mainly recorded visually. The crack widths are mostly estimated based on experience or sometimes measured with a crack width ruler. This results in an error-prone and time-consuming process. Innovative technologies, such as distributed fiber optic sensing, but also methods for digital inspection with mobile devices or photogrammetric survey with unmanned aerial vehicles (UAVs)[14] combined with automated damage detection based on convolutional neural networks (CNNs),[15] have a large potential for the assessment and preservation of an aging infrastructure.

1.2 | Potentials of fiber optic sensing and aim of this study

Due to its ability of measuring strains continuously along the distributed fiber optic sensor (DFOS), fiber optic sensing technology has recently received a lot of attention in the field of experimental research[16–18] and SHM.[19,20] By integrating DFOS into the concrete, it is possible to gain valuable insights into the specimen.[21–23] First approaches to practical applications of crack monitoring, for example, on tunnel shells[24–26] or on bridges,[27–30] have already been carried out. Cracks on concrete structures can be detected by strain peaks, localized with high spatial resolution and crack widths can be determined.[31–33] Based on periodic measurements, the long-term crack development can be analyzed. In addition, extrapolation methods, for example, based on machine learning approaches,[34] enable the prediction of crack widths so that maintenance measures can be planned before the crack has a negative impact on the durability of the structure.

Despite extensive investigations, open research questions remain in the area of crack monitoring for subsequently installed DFOS on existing structures. The chosen DFOS type must be sufficiently sensitive to reliably detect cracks and at the same time have a certain flexibility so that a fiber breakage can be prevented when cracks form. Especially when used under construction site conditions, a certain robustness of the DFOS is required. To ensure reliable long-term monitoring, requirements are also placed on the durability of the DFOS.[35–37]

The aim of this study is to investigate the performance of a DFOS-based crack monitoring on existing structures. Two aspects are of extraordinary importance here: the choice of DFOS type and application technique. To analyze these influences on the strain signal and the calculated crack width, an experimental program was devised in which five different DFOS types were subsequently installed on two large-scale reinforced concrete (RC) beams loaded at service load level in a 4-point bending test. Both filigree as well as robust DFOS, suitable for use on construction sites, are deployed. DFOS were bonded either directly on the concrete surface or along a groove.

In the case of multiple cracks, where the crack spacing is small, crack-induced strain signals will overlap. It is examined whether the widths of closely spaced cracks can be calculated with sufficient accuracy by integrating over the strain course.[31–33,38] Because the DFOS were bonded to the surface of the specimens, direct comparability with reference measurements, such as digital image correlation (DIC) and strain gauges (SGs), is given. When using DFOS, large amounts of data are generated due to the high spatial resolution. To obtain useful information directly, the data must be automatically analyzed and evaluated. Therefore, based on these tests, a PYTHON framework was developed and made freely available.[39]

2 | DISTRIBUTED STRAIN SENSING WITH DFOS

2.1 | Measurement principle

The fiber optic sensing technology is based on the analysis of light backscattering that occurs along the optical fiber. In general, three types of light scattering can be distinguished, namely Rayleigh, Brillouin, and Raman.[19,20,40] Brillouin scattering, measured by means of BRILLOUIN optical time domain reflectometry (BOTDR), and Rayleigh scattering, measured by coherent optical frequency domain reflectometry (c-OFDR), are sensitive to external thermal and mechanical strain changes, allowing the use for distributed temperature sensing (DTS) and distributed strain sensing (DSS). As it is indistinguishable whether strains are due to mechanical or thermal influences, compensation of thermal influences are necessary for mechanical strain measurements under varying temperatures and vice versa.[41] Brillouin scattering-based devices allow measurements with extended ranges up to many kilometers with the trade-off of relatively low spatial resolution (gauge lengths starting from 200 mm).[29] Therefore, Brillouin scattering is mainly used for monitoring linear structures like roads, dams or long tunnels. Devices using Rayleigh scattering currently allow a maximum measurement length up to 100 m, but with a much higher spatial resolution (gauge lengths as low as 0.65 mm), making it the ideal choice for crack monitoring. In construction industry, Raman scattering is mainly used to measure temperature profiles over longer distances with a spatial resolution of up to 50 cm.[42,43] Therefore, it can be used for temperature compensation for Brillouin and Rayleigh measurements.

2.2 | Influence of DFOS type and application technique

Despite the progress in SHM with DFOS and several examples of field applications, challenges still exist in the accurate calculation of crack widths for RC structures. DFOS consist of a core, a surrounding cladding and a coating. The glass core is the central part of the sensing element where the light is transmitted. The cladding layer has a lower refractive index to keep the light signal within the core. To protect the fiber from mechanical impact, a coating is applied. Depending on the requirements for robustness and durability, further protective layers can be provided (e.g., buffer or jacket). The design of the DFOS has a major influence on the strain signal. The magnitude of the measured strains depends on both the shear deformations in the individual layers (and the adhesive), as well as possible slippage between the layers.

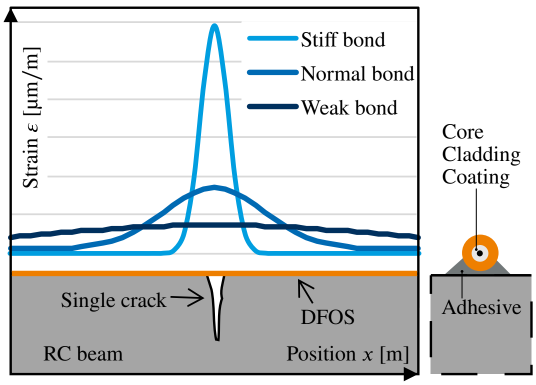

FIGURE 2 Theoretical strain curves for different bond stiffnesses (left); cross-section of a distributed fiber optic sensors (DFOS) on the concrete surface (right).

The measured strain curves are therefore attenuated to some extend depending on the DFOS-adhesive combination and differ from the actual strains in the host material, see Figure 2.

The choice of coating material strongly influences the strain transfer mechanisms and the durability of DFOS.[44] Polyimid (POL), acrylate (ACR), or polyamid/nylon (NYL) coatings are commonly used for laboratory tests. POL forms a chemically bond to the cladding, which enhances the shear transfer.[45] Because of the high stiffness, it can be used where high measurement accuracy is required.[46,47] However, the low durability in the alkaline milieu of the concrete is problematic, which causes the degradation of the coating and can lead to signal loss.[35] Alternatively, an ORMOCER® (ORM) coating can be chosen, which has a similarly stiff strain transfer[48,49] but significantly better properties in terms of durability.[36] In the area of cracks, where large strain gradients occur, the choice of more flexible coating materials, such as ACR or NYL, can be favorable. Strain peaks are attenuated to some extent, thereby reducing the risk of DFOS failure. To increase robustness against mechanical impact and reduce the risk of damage during installation, the DFOS can be protected by additional layers (e.g., by a plastic or metal jacket).

For monitoring from zero hour, it is recommended to integrate the DFOS directly into the component. The DFOS can either be embedded in the concrete matrix[30,50,51] or attached to the reinforcement.[52–54] For existing structures, the DFOS must be installed subsequently, whereby a stiff bond between the component and the DFOS must be ensured for reliable strain measurement. DFOS can be glued either directly on the prepared concrete surface or along a milled groove (near-to-surface installation).[28,29,55,56]

It must be considered that the choice of adhesive further influences the strain transfer.[49,57–59] In previous experimental research, a variety of adhesives have been utilized, such as the commonly used cyanoacrylate adhesive, epoxy resin, silicone, urethane, and injection mortar. Due to their high stiffness as well as chemical and weather resistance, epoxy adhesives or injection mortars are well suited for the subsequent installation of DFOS on concrete components. For practical applications, such as overhead installation, the curing time and viscosity also play an important role. In addition, adhesives with a low shrinkage behavior are recommended, since shrinkage cracks in the adhesive matrix complicate the interpretation of the measurement data.

2.3 | Experimental investigations on crack monitoring with DFOS

Due to the complex interaction between the optical fiber and the concrete component, it is advisable to test the suitability of a particular DFOS type and its application method before using it on real structures. For this reason, numerous experimental studies were conducted to investigate the viability of a Rayleigh-based DSS with various DFOS types and adhesives for crack monitoring on RC structures.[31,32,60–62] In the following, individual experiments are presented in which the DFOS were either embedded in the concrete matrix or subsequently installed on the specimens.

In 2012, Henault et al.[51] carried out 4-point bending tests on RC beams, where they both embedded DFOS within the concrete matrix and bonded them to the surface. The surface-bonded DFOS had the form of an adhesive tape, with the controlled thickness of the adhesive layer ensuring homogeneous bonding along the DFOS' length. It has been shown for the first time that it is possible to detect and localize appearing cracks much earlier than visual inspection.

Regier and Hoult[63,64] tested a series of small RC beams and found that NYL-coated DFOS glued with a two-part epoxy adhesive to the concrete surface were able to bridge crack openings without breaking. However, the relatively soft coating and possible slippage poses the risk that two closely spaced cracks appear as a single strain peak.

Villalba and Casas[65] glued stiff POL-coated DFOS with a cyanoacrylate adhesive on a RC slab, which was subjected to a bending test. It was shown that the DFOS was able to detect the appearance of cracks that were hardly visible. Surprisingly, despite the stiff coating, it was possible to perform strain measurements up to crack widths of 1.0 mm. Based on these experiments, a method for determining the mean crack width by integrating the strain curve was later presented.[61] An acceptable agreement was found between the displacement transducer and the calculated crack widths.

In further studies by Barrias et al.[66] and Fischer et al.,[31] accurate results could be achieved in the elastic state with a POL-coated DFOS on the concrete surface. However, the risk of fiber breakage increased with the crack formation. This risk can be reduced by choosing a soft adhesive, so that the amplitude of crack-induced local strain peaks can be attenuated.[53,59] The deployment of DFOS with a stiff coating can be a good choice for monitoring shear performance of concrete structures where the primary concern is the detection of the onset of crack formation rather measuring larger crack widths.[67]

In the aforementioned study by Fischer et al.,[31] with NYL-coated DFOS bonded with a cyanoacrylate adhesive, clear strain curves with pronounced strain peaks in the area of crack openings were obtained. In comparison, other robust DFOS that can be used under harsh site conditions were investigated. Depending on the DFOS design, there were distinct differences in the strain curves. Compared to the NYL-DFOS, the robust DFOS showed a softer bond behavior with a damped strain curve and much smaller strain peaks. In addition, a methodology is presented schematically to calculate individual crack widths based on the strain curve and taking tension stiffening (TS) into account.

Brault and Hoult[33] conducted 3-point bending tests on 13 RC beams with the objective to monitor deflections and cracks with NYL-coated DFOS bonded to the concrete surface with epoxy adhesives. Different methods for the crack width calculation based on the strain curves were proposed and evaluated in terms of their accuracy using DIC as a reference measurement. It was found that the DFOS could measure crack widths with an average measurement difference 0.031 mm for crack widths between 0.18 mm and 0.30 mm.

Bednarski et al.[29] and Howiacki et al.[30] carried out 4-point bending tests on 4 m long RC beams, focusing on the performance of various robust DFOS embedded in the concrete matrix. DFOS with a multilayer and monolithic cross-section were compared. It was found that the monolithic DFOS exhibits a much stiffer strain transfer. The damped strain curve of the multilayer DFOS was attributed to possible slippage between the layers. The crack widths were estimated using a simplified approach via strain integration and showed a good agreement with the reference measurement.

Experimental investigations on a notched, prestressed beam on the influence of the DFOS type and the application technique were also carried out by Vorwagner et al..[56] Good results were obtained with a "tight buffered" DFOS bonded directly to the concrete surface with an epoxy-based anchor adhesive. Strains could be measured reliably even up to crack widths of 2.6 mm. However, at unloading, the strain peak reversed with a plastic strain component, which was attributed to slippage between the layers. The authors used this artifact to calculate the maximum crack width occurred in the past based on a numerical model.

Also in tests by Novák et al.[28] a robust DFOS with an ethylene–propylene protective layer bonded with a mineral-bound adhesive in a groove provided reliable strain measurements. Closely neighboring cracks with crack spacings of less than 10 cm could be reliably detected by individual strain peaks. However, at crack widths greater than 0.6 mm, slippage occurred.

Due to the numerous influencing parameters, it is not possible to provide a general conclusion on the choice of the right DFOS and the application technique (adhesive type, surface vs. near-to-surface installation) for crack monitoring on RC structures. However, trends can be derived from the investigations carried out: If strains are to be measured with high accuracy in the non-cracked state, a DFOS with stiff POL or ORM coating seems predestined.[49,66] However, with the onset of crack opening, a certain amount of flexibility is required to prevent fiber breakage. For measurements in the cracked state, DFOS with a softer coating (e.g., made of NYL) are therefore advantageous.[31,64] While additional protective layers increase the robustness and durability of the DFOS, there is a risk that the strain peaks will be strongly attenuated due to slippage between the layers.[29,30,50]

2.4 | Strain transfer mechanisms

In the past, several theoretical models were developed to describe the complex strain transfer mechanisms that relate the strain from the host material to the DFOS core. Her and Huang[58,68] carried out experimental investigations on the effect of coating and adhesive and developed an analytical model for continuous strain fields. The problem of strain transfer is exacerbated in the area of strain singularities (i.e., cracks).[51,69] Bassil et al.[70] generalized Feng's model[69] to a multilayer system taking imperfect bonding between the layers into account. The introduced "strain lag parameter" can be used to calculate the crack openings on the basis of the maximum strain value. This parameter can either be determined theoretically or experimentally. However, wedge-splitting tests showed that the proposed model yielded to large errors for robust DFOS with a protective metal tube around the optical fiber. Alj et al.[59] developed a finite element model to describe the strain transfer for thick-coated DFOS glued in a groove on the concrete surface. Based on this, an analytical approach is proposed relating a DFOS strain peak to the crack opening. However, this approach is valid only in the elastic domain of materials and bond relationships.

2.5 | Crack width calculation for DFOS

Because of the uncertainties associated with the analytical models, for example, unknown geometric and mechanical

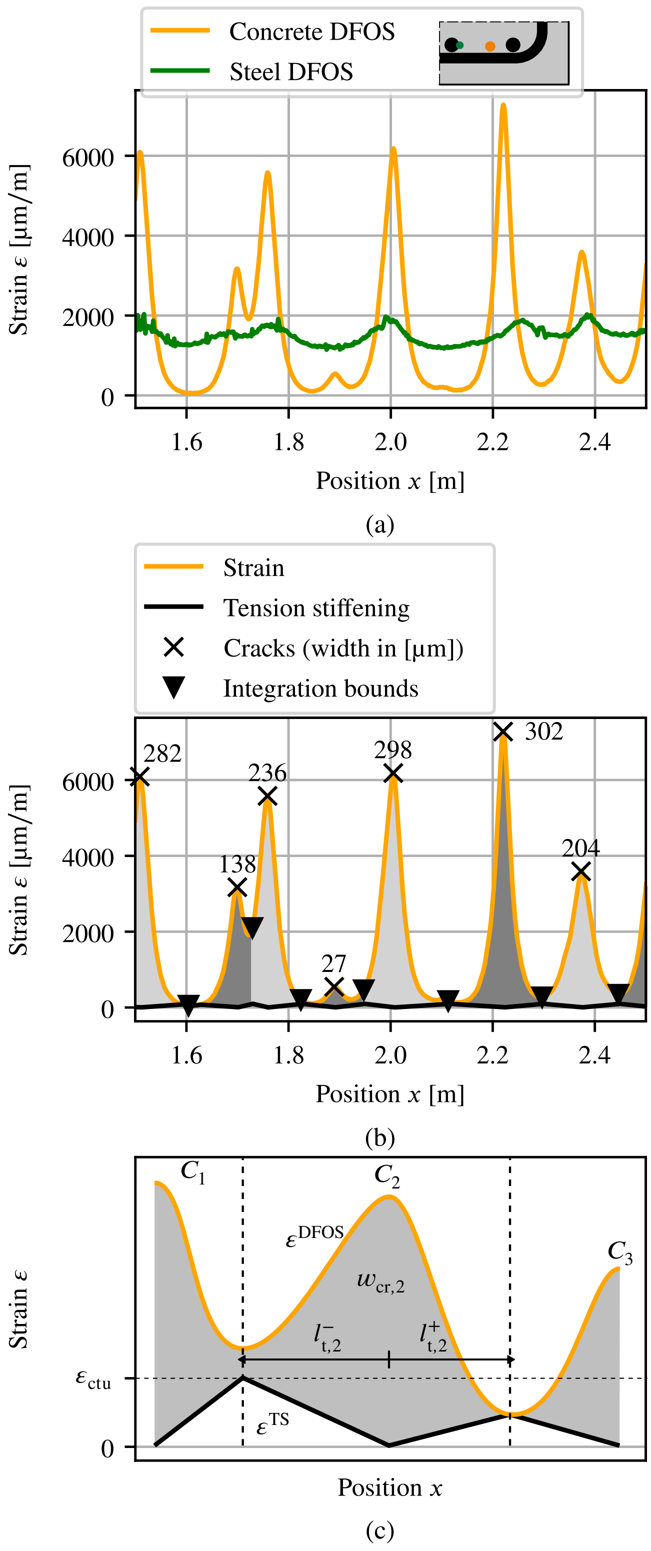

FIGURE 3 Crack width calculation schemes for concrete distributed fiber optic sensors (DFOS). (a) Strain curves for concrete and steel DFOS, **(b)** Crack width calculation for concrete DFOS, and **(c)** Schematic representation for compensating TS strains.

properties of the individual layers as well as nonlinear interactions between the layers, a graphical interpretation of the strain curves is generally preferred for crack width determination.[31–33,38] In the design codes,[71,72] the calculation of the crack width w_{cr} is based on mechanical models and defined as

$$w_{cr} = s_{r,\max}(\varepsilon_{sm} - \varepsilon_{cm}), \tag{1}$$

where $s_{r,\max}$ is the maximum crack spacing and ε_{sm} and ε_{cm} are the mean steel and the mean concrete strain, respectively.

Figure 3a shows the differences in the strain curves for DFOS embedded in the concrete matrix and for DFOS bonded to the reinforcement (hereafter referred to as concrete and steel DFOS). While the concrete DFOS shows pronounced strain peaks in the cracked cross-sections, the basic strain level of the steel DFOS depends largely on the applied bending moment, which is why the strain amplitudes are significantly lower. This fact already indicates the high suitability of concrete DFOS for crack detection and localization.

With regard to Equation (1), strains in the reinforcement can be measured well using DFOS. While the theoretical concrete strains are zero in the area of the crack openings, the DFOS is bridging the crack, showing pronounced strain peaks. The general Equation (1) can therefore not be used. Instead, as illustrated in Figure 3b, the crack width can be determined by integrating the strain curve of the concrete DFOS. The width $w_{cr,i}$ of the ith crack is equal to the integral of the DFOS strain $\varepsilon^{DFOS}(x)$ along the transfer length l_t:

$$w_{cr,i} = \int_{x_{cr,i} - l_{t,i}^{-}}^{x_{cr,i} + l_{t,i}^{+}} \varepsilon^{DFOS}(x) - \varepsilon^{TS}(x)\,dx \tag{2}$$

with x_{cr} as the crack location, l_t as the transfer length, and $\varepsilon^{TS}(x)$ as the part of strains resulting from TS. The location of the crack x_{cr} is determined by means of peak finding.[39] The transfer length l_t is assumed to be equal to half of the crack spacing. Another approach is to consider the distance to the neighboring minima as the transfer length. However, the first approach is more stable on erratic behaving strain data as it is less prone to noise-induced minima. It is important to mention that both approaches are only applicable at the stabilized crack stage. Otherwise, the transfer length for the individual cracks would be significantly overestimated, which in return would lead to an overestimation of the crack width. For the crack formation stage, when first cracks appear, the transfer length must be limited reasonably.

Away from the crack opening, tensile forces are reintroduced into the concrete by bond interactions with the reinforcement. This is the reason why, with increasing distance from the crack, a small part of the measured strain is due to TS, which has to be compensated by the subtrahend $\varepsilon^{TS}(x)$. Different approaches for the influence of TS are present in the literature. It needs to be differentiated between concrete[31,33] and steel DFOS.[32] Fischer et al.[31] proposed an approach for crack width calculation for DFOS embedded into the concrete or attached to the concrete surface. The basic principle is illustrated in Figure 3c. TS is simplified and assumed to increase linearly from 0 at the crack position to the maximum tensile strain of the concrete ε_{ctu} at the border of the crack's transfer length:

$$\varepsilon^{TS}(x) = \min\left(\delta_{\varepsilon} \times \varepsilon_{ctu}, \varepsilon^{DFOS}\right) \tag{3a}$$

with the constant slope within the transfer length:

$$\delta_{\varepsilon} = \begin{cases} \dfrac{x_{cr} - x}{l_t}- & \text{if } x \le x_{cr}, \\[2ex] \dfrac{x - x_{cr}}{l_t}+ & \text{if } x > x_{cr}. \end{cases} \tag{3b}$$

The maximum tensile strain at the onset of cracking ε_{ctu} can be calculated from the material properties as:

$$\varepsilon_{ctu} = \frac{f_{ctm}}{E_{ci}} \approx 100\ \mu\text{m/m} \tag{4}$$

where f_{ctm} is the mean tensile strength and E_{ci} is the tangent modulus of elasticity.

In this article, crack widths are determined by integrating the strain curves of concrete DFOS. A comparison between the different approaches for concrete and steel DFOS, the influence of TS as well as the effects of this "min"- and "middle"-approach for the determination of the transfer length are discussed in another study.[39]

3 | EXPERIMENTAL INVESTIGATIONS

The goal of the laboratory tests was to identify suitable DFOS, which are able to (a) detect, (b) localize, and (c) measure crack widths with high accuracy within the serviceability limit state (SLS). The focus was on DFOS that can be installed subsequently on the concrete structure and withstand harsh conditions of the construction site. Furthermore, the strain transfer was compared for DFOS bonded either in a groove or directly to the smooth concrete surface. For this purpose, two reinforced concrete beams were loaded in a 4-point bending test under service load level.

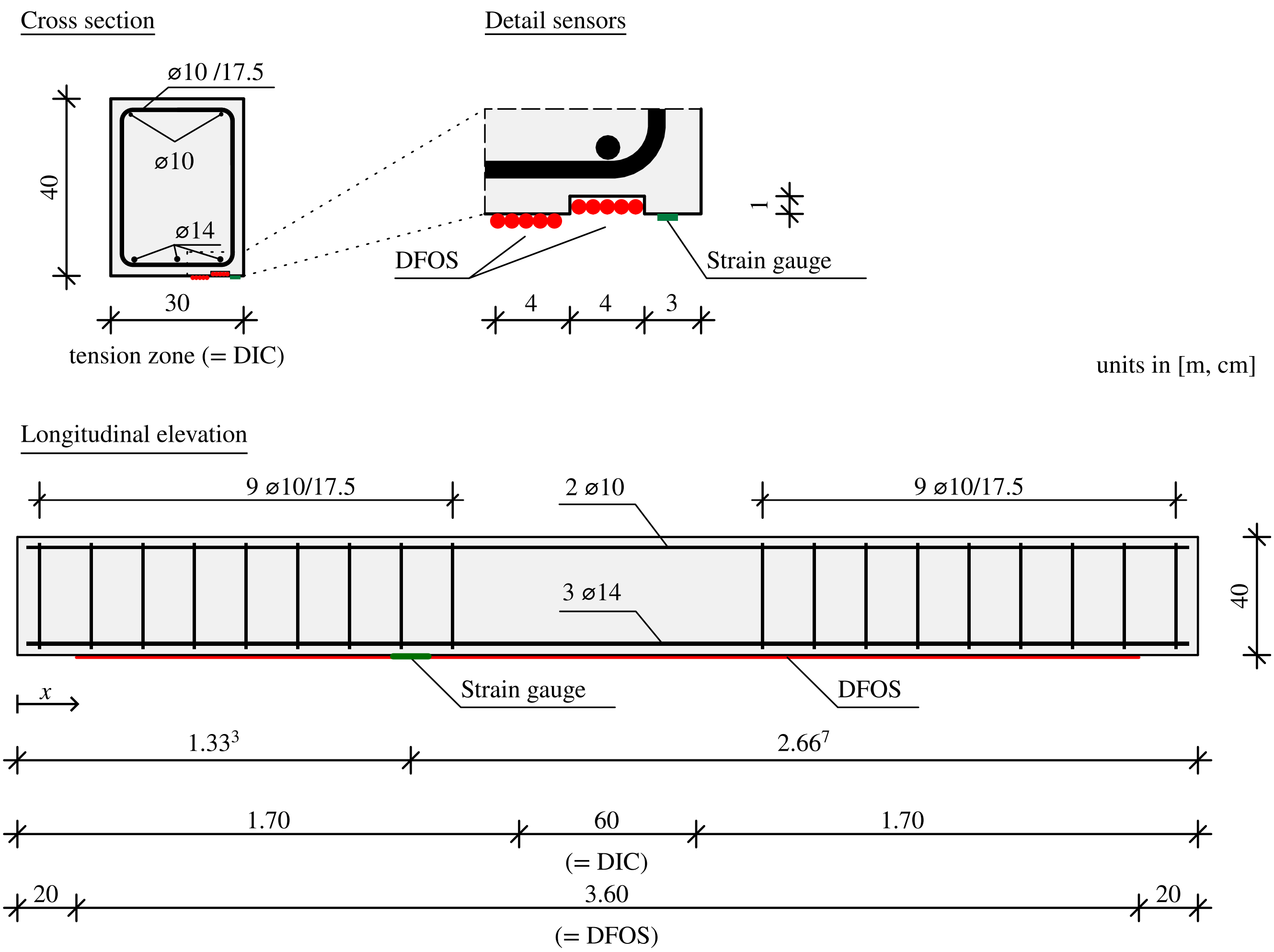

FIGURE 4 Geometry and reinforcement layout of the specimens (here: beam no. 1; beam no. 2 has only five distributed fiber optic sensors (DFOS) bonded into a groove).

3.1 | Specimen geometry and reinforcement layout

The cross-section of the specimens with the reinforcement layout can be seen in Figure 4. The RC beams were 4 m long and had a rectangular cross-section of $b \times h = 30$ cm $\times$ 40 cm. The concrete cover was 20 mm. In order not to influence the crack pattern in the center of the field, stirrups were omitted there (constant bending moment and no shear forces).

3.2 | Materials and sample preparation

For concreting the specimens, a flowable concrete (consistency class F5) C30/37 (cement CEM III/A 42.5N) with a maximum aggregate diameter of 8 mm was used. After concreting, the specimens were covered with a polyethylene sheet to minimize moisture evaporation. Five days after concreting, the formwork was removed

TABLE 1 Material properties for the used concrete mix.

Properties	Mean value [N/mm^2]	CoV [%]	Test acc. To EN 12390-
f_c	42.7	1.9	3
$E_{C,S}$	30,300	2.7	13
f_{ct}	3.08	5.1	6
$f_{ct,fl}$	3.8	9.0	5

and the specimen remained until loading in the same indoor climate (21.0°C ± 2.0°C, 40% RH ± 10% RH). Despite the measures after concreting, first shrinkage cracks could already be identified in the area of the stirrups.

Additional samples for the material tests were stripped after 1 day, then wrapped in moist towels for another 6 days and afterwards stored in the immediate vicinity of the beams until the material tests were carried out 28 days after concreting. Five cylinders ($d \times h = 15$ cm $\times$ 30 cm) each were used

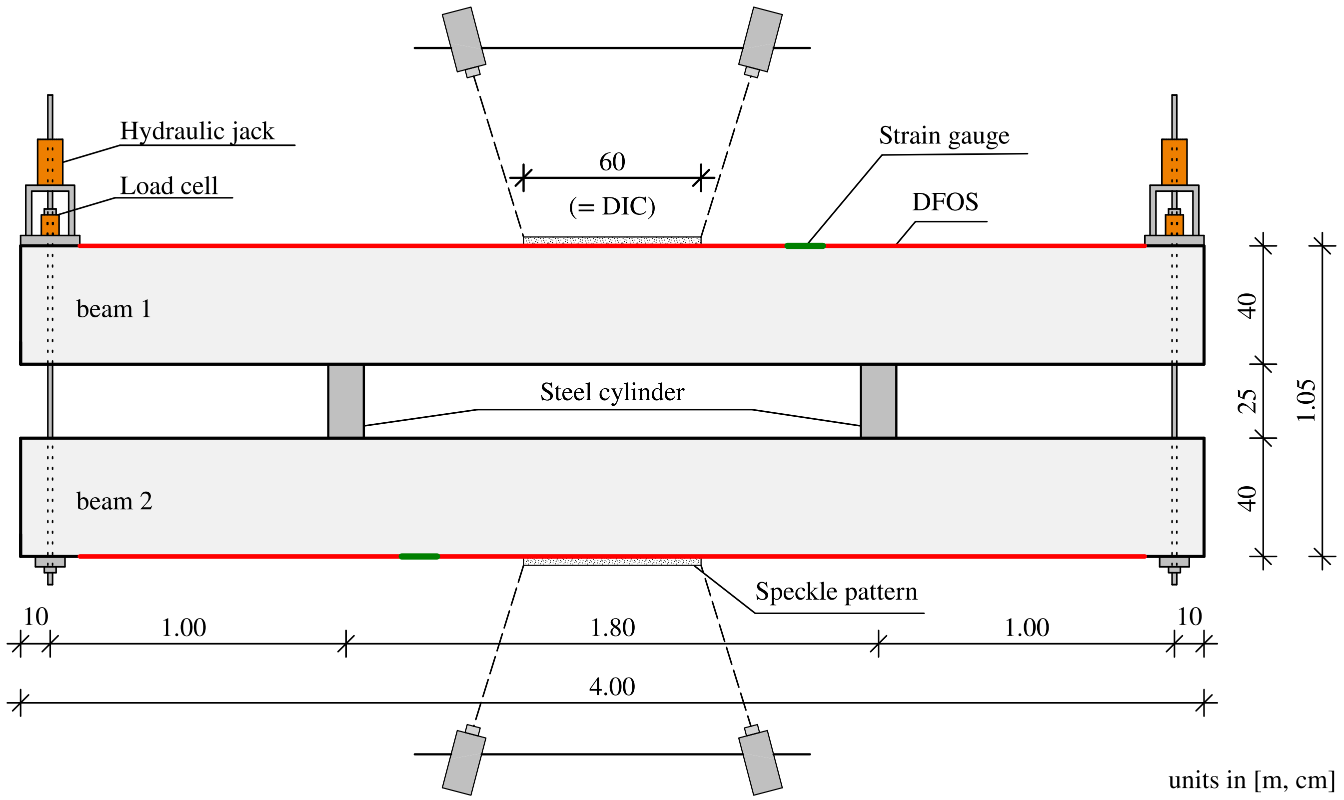

FIGURE 5 Test setup and measurement layout.

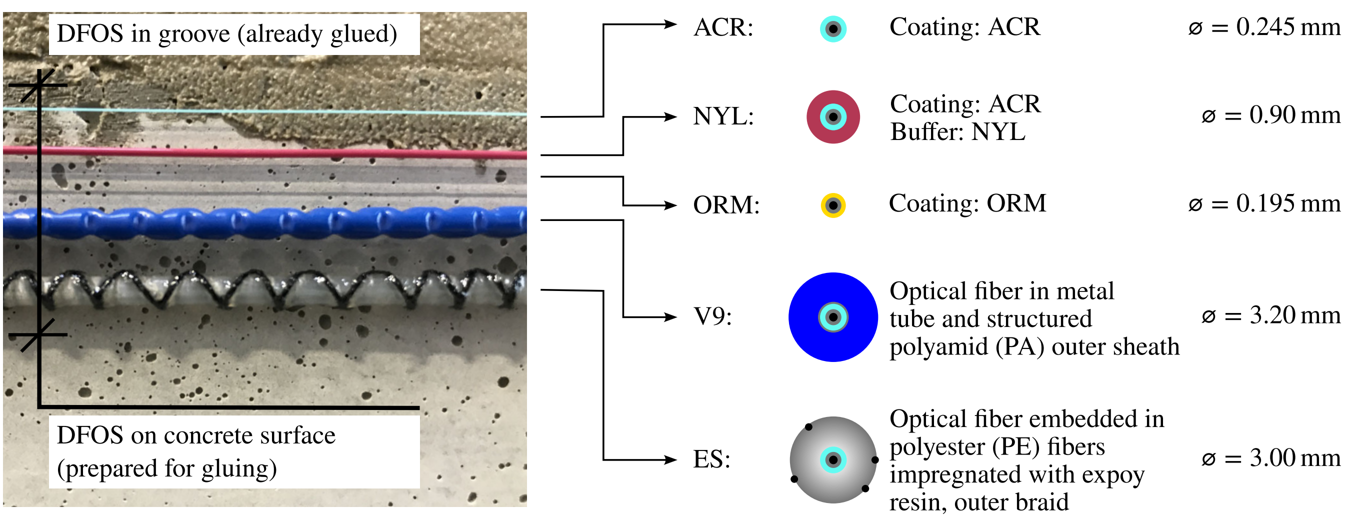

FIGURE 6 Applied distributed fiber optic sensors (DFOS) on beam 1 (left) and their cross sections (right, unscaled).

to determine the concrete compressive strength f_c[73] the Young's modulus $E_{c,s}$[74] and the tensile splitting strength f_{ct}[75] The flexural tensile strength $f_{ct,fl}$[76] was determined using five prisms ($w \times h \times l = 10 \times 10 \times 40$ cm). The results of the material tests are summarized in Table 1. For the reinforcement steel, B500B with yield strength of 500 N/mm^2 was used.

3.3 | Test setup and procedure

The loading took place 29 days after concreting. During the test, the two specimens were kept on distance by steel cylinders as shown in Figure 5, lying on the floor and prestressed against each other at the ends by hydraulic cylinders. Thereby, the loading situation is equal to a

4-point bending test. The tensile zones are on the outer sides of the specimens, so that the crack formation can be well recorded by DIC. In order to reduce the friction between the specimens and the concrete foundation to a minimum, the specimens were bedded on the following layers: talcum powder, polyethylene sheet, talcum powder, polyethylene sheet, cardboard from the corrugated board (from top to bottom). The load was applied within 20 min. After reaching the target load of 50 kN per press, hexagon nuts were fixed in the area of the load cells so that the deflection remained constant over the test period of almost 4 months. This article deals with the measurements during and immediately after loading. Results on the long-term behavior of the DFOS will be published later.

3.4 | Metrology

As shown in Figures 4 and 5, for the measurement electrical SGs, DFOS, and DIC were used. The five DFOS types used in the tests are shown in Figure 6. DFOS with a coating of ORM or ACR are very filigree and have a diameter of less than a quarter millimeter. Note that in Figure 6, the thin ORM-DFOS is almost invisible due to the transparent coating. The NYL-DFOS has a diameter of 0.9 mm and is protected against external mechanical influences by an additional NYL buffer. The robust DFOS, EpsilonSensor (ES), and V9 (V9), have a more complex structure and are well suited for harsh site conditions. In both cases, the outer surface is roughened to improve the bond to the concrete by mechanical interlocking.

Each of these DFOS types was installed in a subsequently cut groove on both beams (near-to-surface installation). The installation in a groove appears to be advantageous in many aspects: protection of the DFOS against weathering and mechanical impacts, increase of the active bonding surface (three-sided instead of one-sided bond to the existing structure), more reliable temperature measurement, higher aesthetics. A disadvantage, however, is the increased time and effort required to produce the groove. In order to be able to evaluate the necessity of the groove, for beam 1, the DFOS were additionally glued directly onto the smooth concrete surface, cf. Figure 6. Before gluing, the concrete surface was only cleaned of dust and coarse dirt.

During installation, the DFOS were first fixed in position point by point, then the adhesive was applied and finally smoothed out with a spatula. In order to be able to systematically analyze the influence of the DFOS type and the application technique, all DFOS were bonded with the same adhesive. For the tests, a fast-curing two-component injection mortar with a resin component was used. The short processing time of only a few minutes and high viscosity enables overhead bonding of DFOS on existing structures.

In total, 15 DFOS were applied (each DFOS type 2× in a groove and 1× on the concrete surface). Already before loading, one ACR-DFOS on the surface of beam 1 failed. Also, the ORM-DFOS at beam 2 showed an unrealistic strain distribution with an almost constant strain plateau over a length of about 1.5 m. As a result, only 13 out of the 15 DFOS were available for the evaluation.

For the measurements, the optical distributed sensor interrogator (ODiSI) 6100 from Luna Inc. was used as a data acquisition unit. In order to be able to detect microcracks as well, the highest spatial resolution available was used. Accordingly, the distance between the measuring points was set to 0.65 mm. During loading, the two robust DFOS (ES and V9) on beam 1 were measured with a sample rate of 1 Hz. Directly after reaching the target load level, the remaining DFOS were each measured for a period of about 30 s.

In comparison, the crack propagation in the tensile zone in the field center was captured via DIC over a length of 600 mm. Therefore, the commercial system GOM ARAMIS® with a stereo camera system with 12 Mpixels resolution (4000 × 3000 pixels), was used. The system was calibrated for a measuring volume of 605 × 465 × 465 mm. According to the calibration protocol, the deviation was 0.018 pixels, which corresponds to a theoretical accuracy of 2.7 μm with the existing measurement volume and the camera resolution.

Local concrete strains were also measured with one SG for each beam. The SGs had a gauge length of 120 mm and were glued onto the prepared concrete surface.

4 | TEST RESULTS

4.1 | Strain development during loading

First, the strain development during loading for the robust DFOS, ES, and V9, is presented for beam 1. Figure 7 shows the strain distribution over one half of the beam length at three different load levels: $0.5F_{cr}$, $1.0F_{cr,}$ and $2.0F_{cr}$, where the cracking force F_{cr} was calculated with the characteristic concrete tensile strength $f_{ctk} = 0.7f_{ctm}$.

To verify the DFOS strains, a local SG measurement is used. During loading, a crack occurred at the location of the SG. In addition, the strain curves are compared with the theoretical strain distribution according to the elasticity theory. The strains in the tensile zone of the uncracked beam are calculated as follows:

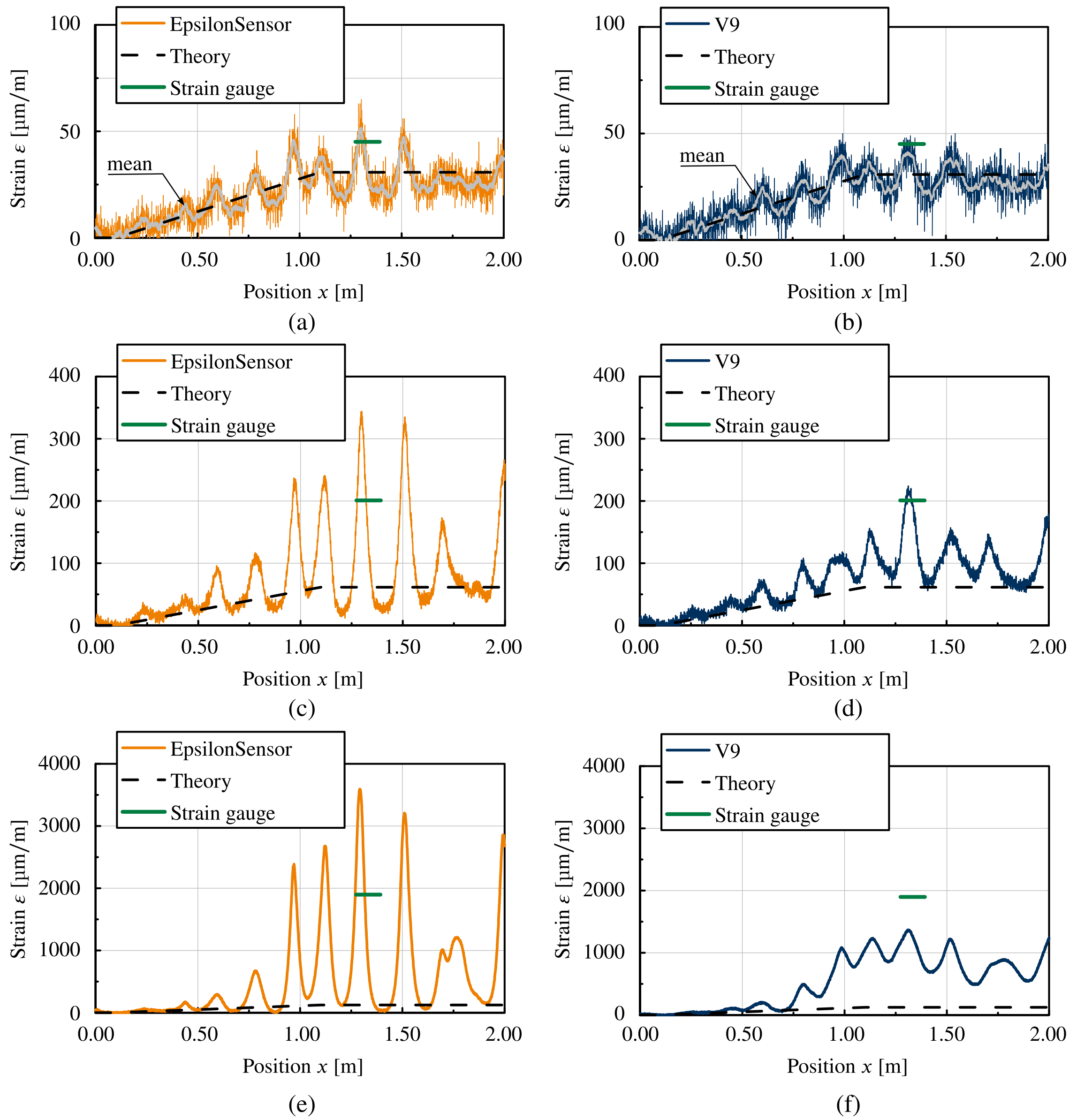

FIGURE 7 Strain profiles for three different load levels along one half of beam 1 measured with robust distributed fiber optic sensors (DFOS) (ES and V installed in a groove). (a) ES for $F = 0.5F\mathrm{cr}$, (b) V9 for $F = 0.5F\mathrm{cr}$, (c) ES for $F = 1.0F\mathrm{cr}$, (d) V9 for $F = 1.0F\mathrm{cr}$, (e) ES for $F = 2.0F\mathrm{cr}$, and (f) V9 for $F = 2.0F\mathrm{cr}$.

$$\varepsilon_c(x) = \frac{M_y(x)}{E_c I_y{}^*} z \tag{5}$$

where $M_y(x)$ is the in-plane bending moment, z is the distance to the neutral axis and E_c is the modulus of elasticity of the concrete as listed in Table 1. The ideal moment of inertia $I_y{}^*$ considering the different material stiffnesses can be determined according to Equation (6):

$$I_y{}^* = I_c + A_c d_c{}^2 + (\alpha_e - 1) A_s d_s{}^2 \tag{6}$$

where I_c is the moment of inertia of the pure concrete section, A_c is the gross cross-sectional area of the concrete, A_s is the area of the reinforcement, $\alpha = \frac{E_s}{E_c}$ is the ratio of Young's moduli and d_c respectively d_s are the distances between the neutral axis of the transformed section and the centroid of the concrete or reinforcement.

At a low load level ($0.5F_{cr}$), both DFOS types showed a relatively good agreement with the SG measurements as well as with the theoretical strains according to the elasticity theory. It is noticeable that despite the low load level, far below the cracking force, first strain peaks could be observed. As mentioned before, shrinkage cracks appeared in the area of the stirrups despite the concrete curing measures. The crack opening could be monitored accurately. Also in the mid-section, where no stirrups were placed, a first strain peak at $x = 2.0$ m became

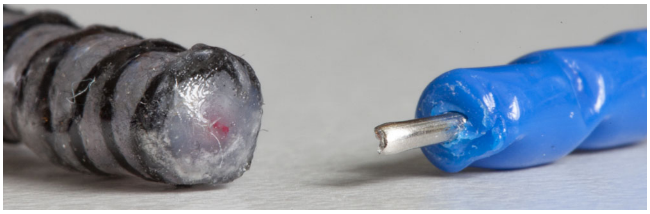

FIGURE 8 Structure of robust distributed fiber optic sensors (DFOS): ES (left) and V9 (right).

apparent. In the range of low strains, the measurement noise level of about $\pm 10\,\mu\text{m/m}$ was visible, which corresponds well with the information from the ODiSI manual.[77] The noise depends on the choice of the gauge length and increases with finer measurement resolution. For the low load level, part of the noise was reduced by a moving average with a sliding window interval $[x_{i-10}, x_{i+10}]$ for the current position i. For all other graphs, the raw strain curves are presented.

At $1.0F_{\mathrm{cr}}$, it could be clearly seen how two cracks opened in the center of the field. The strain profile of the ES showed pronounced local strain peaks in the area of the cracks, which ensures that the onset of crack formation can be reliably detected.

With further load increase to $2.0F_{\mathrm{cr}}$, these differences between the strain curves became more apparent. While the ES measured a maximum strain of $3500\,\mu\text{m/m}$, the strain profile for the V9 was strongly damped with not even half as high maximum strains. Between the cracks, the strains of the V9 were much higher than the maximum possible tensile strains $\varepsilon_{\mathrm{ctu}}$. Regardless of the qualitative strain profile of the two DFOS, the area below the curves and thus the calculated elongation was approximately the same (for $2.0F_{\mathrm{cr}}$ and $1.5\text{ m} \leq x \leq 2.5\text{ m}$: $\Delta L_{\mathrm{ES}} = 0.78$ mm and $\Delta L_{\mathrm{V}} = 0.76$ mm).

It is supposed that the damped strain curve of the V9 resulted from the layered structure of the DFOS, see Figure 8. As the load increases, slippage between the layers probably occurred, especially in the regions of high strain gradients. The ES, on the other hand, convinced with a stiff strain transfer due to its monolithic structure. Combined with the relatively low axial stiffness, even fine cracks could be detected with a high reliability at the crack formation stage.

4.2 | Influence of the DFOS type

In the following, the strain curves and calculated crack widths for the different DFOS are compared with those of DIC. Figure 9a shows the crack pattern and strain distribution of the DIC measurement on beam 1 along the measuring length of 60 cm. In the crack openings (absence of concrete), the strains approach infinity and decrease to almost zero in the uncracked regions. The crack openings were determined with GOM Correlate using a virtual extensometer at the level of the DFOS. Four cracks ($C_{1,\ldots,4}$) with a width of 0.17 mm to 0.34 mm were recorded. In addition, a smaller crack, labeled as microcrack (M_1), with a width of 0.03 mm was detected at the same height as the DFOS. In Figure 9, these strain curves and crack widths are used as a reference for the DFOS measurements made in the groove of beam 1. The crack widths w_{cr} for the DFOS were determined, as presented in Section 2.5, by an integration of the strain curves, using the half crack spacing as the integration boundaries. For comparability, the same procedure was used for all DFOS. Only the prominence for crack detection had to be defined DFOS specific and varied from $100\,\mu\text{m/m}$ for DFOS with clear strain curves without outliers (e.g., ES and V9) to $2000\,\mu\text{m/m}$ for the stiff ORM-DFOS. A too low prominence leads to incorrect crack identification in the case of unsteady strain curves.[39] The influence of TS was taken into account, but is generally small as the following numerical example shows: For cracks with a spacing of 0.2 m and a maximum tensile strain $\varepsilon_{\mathrm{ctu}}$ of $100\,\mu\text{m/m}$, the crack width is reduced by 0.01 mm, which is marginal in view of the usual crack widths in the range of 0.2 mm to 0.4 mm in the SLS. In addition, neglecting TS would be on the safe side.

Figure 9b to f shows the strain curves of the different DFOS, sorted from relatively soft to stiff strain transfer. In Figure 9b, once again the strongly attenuated course for V9 is evident. As a result, the two adjacent cracks at $x \approx 1.75$ m were interpreted as one crack, which led to a significant overestimation of the crack width ($w_{\mathrm{cr,DFOS}} = 0.43\text{ mm} \gg 0.26\text{ mm}$ resp. 0.17 mm). Note that the sum of the two individual cracks measured by DIC is equal to the calculated crack width of 0.43 mm. For the other two cracks identified as such via individual strain peaks, the calculated crack widths agreed well with DIC.

The NYL-DFOS in Figure 9c also showed a largely damped strain curve, which was probably caused by slippage between the ACR-coating and the NYL-buffer. Although all cracks have been detected, precise localization can be problematic.

A proper strain transfer was observed for the ES, see Figure 9d. Except for the microcrack M_1, all cracks could be detected. The cracks are characterized by pronounced strain peaks and could therefore be localized with high accuracy. The calculated crack widths agree almost perfectly with the reference measurement.

Also the ACR-DFOS in Figure 9e is characterized by a stiff bond with pronounced strain peaks in the area of

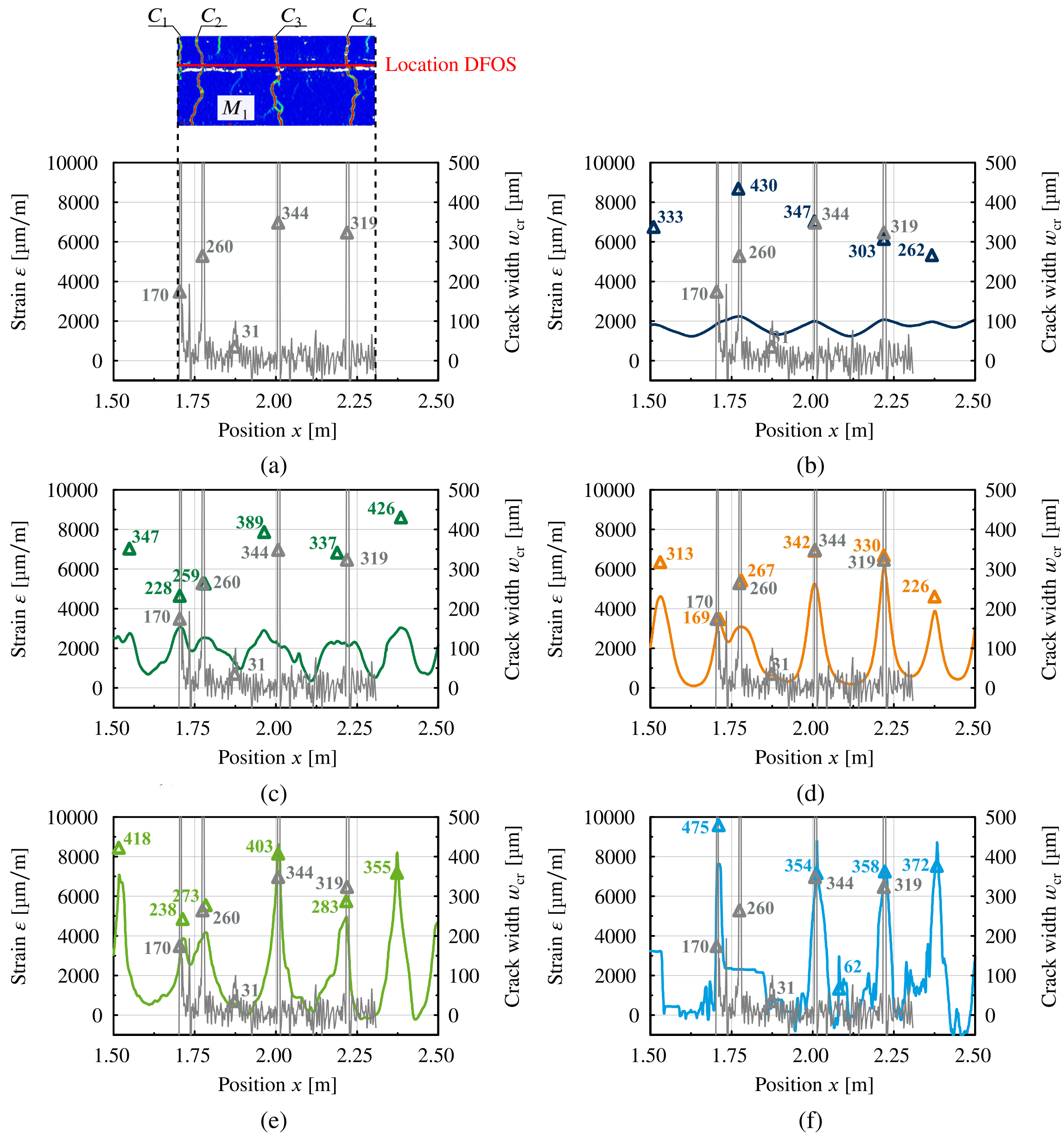

FIGURE 9 Results for crack monitoring using various distributed fiber optic sensors (DFOS) (here: beam 1, DFOS glued into the groove). (a) Digital image correlation (DIC), (b) V9 (V9), (c) polyamid/nylon (NYL), (d) EpsilonSensor (ES), (e) acrylate (ACR), and (f) ORMOCER® (ORM).

the cracks. Despite a precise crack localization, the calculated crack widths fluctuate around the DIC measurement with a higher measurement deviation compared to the ES.

The ORM-DFOS in Figure 9f showed the stiffest strain transfer with steep strain peaks and high strain gradients. Unlike the ACR-DFOS, however, there is an irregular or jagged course between the cracks, which can lead to strain peaks being incorrectly recorded as cracks. For example, at $x \approx 2.1$ m a crack was detected that does not exist according to DIC measurement. How to deal with such jagged strain curves in the evaluation is discussed in another study.[39] The crack widths at $x \approx 2.0$ m and $x \approx 2.25$ m could be well represented. Two strain plateaus appeared along the measuring length (at $x \approx 1.5$ m and $x \approx 1.8$ m), which, in case of the second plateau, resulted in two cracks being detected as one. Thus, the crack width was clearly overestimated.

It should be noted that the DFOS were glued over a height of about 6 cm in the tension zone of the beam and the crack widths from DIC were always measured in the center of the DFOS (at the height of the red line in Figure 9a). The crack widths were not constant over their length. However, it could be proven that in the relevant

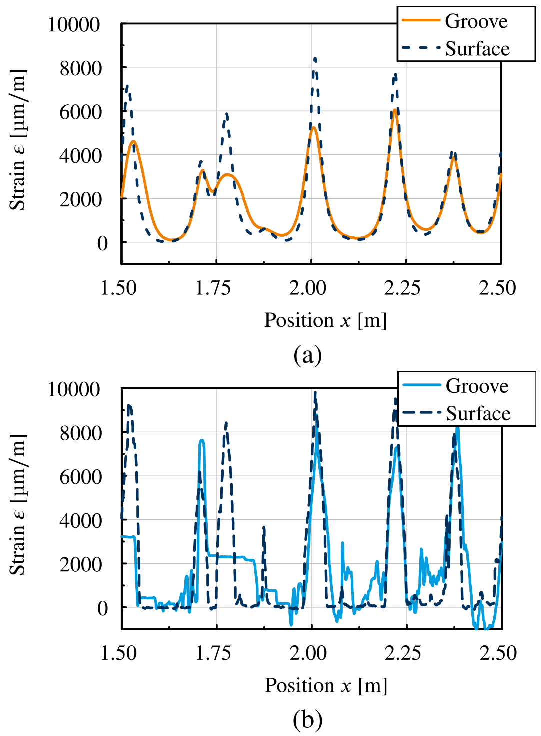

FIGURE 10 Influence of application technique on the strain distribution for (a) ES and (b) ORM-distributed fiber optic sensors (DFOS).

range of ±3 cm the influence of variable crack width was negligible.

4.3 | Influence of the installation method

While for new structures (monitoring from "zero hour") DFOS can be installed in the formwork before concreting, for existing structures the only option is to bond the DFOS subsequently to the component. Since only the changes in crack widths can be measured when monitoring existing structures, an initial measurement must be carried out to determine the absolute crack width.

In the following, it is discussed whether a reliable bond to the concrete component can also be achieved with a subsequent DFOS installation. The strain curves for the ES and the ORM-DFOS are compared exemplarily in Figure 10. It can be seen that for the DFOS that were subsequently bonded to the surface, a good strain transfer took place, despite the smooth concrete surface and the smaller bonding surface (one-sided bonding). The strain peaks were even larger than those of the DFOS, that were bonded into the groove. A small part of the strain increase can be explained by the larger inner lever arm z, although the groove depth was only 1 cm. Except for the V9, even the microcrack at $x \approx 1.88$ m could be detected with all other DFOS on the surface.

With the ORM/DFOS glued to the surface, the strain curve between the cracks was much clearer. The groove was made with a flex and a hammer drill, so that there was a rough surface on the inside. It is assumed that the unsteady course of the ORM-DFOS bonded in the groove can be attributed to this rough surface and the resulting transverse pressures. With the ORM-DFOS on the surface, both closely adjacent cracks at $x \approx 1.75$ m could be detected clearly. Between the cracks, there were almost strain-free sections.

The observed strain plateaus for the ORM-DFOS in the groove can be attributed either to slippage within the DFOS or within the bond zone. Since the measurements on the concrete surface showed even higher strain peaks and no measurement anomalies were found there, slippage within the bond zone is suspected. For an installation of ORM/DFOS within a groove, an adhesive with a lower viscosity would probably be beneficial to ensure a continuous and homogeneous bond to the component.

Due to the stiffer bond behavior, the ORM-DFOS has a much shorter transfer length than the ES. Thus, the ORM-DFOS offers also potential for crack monitoring on components with a finer distributed crack pattern, such as carbon-reinforced concrete structures.

The influence of the installation technique on the calculated crack width was marginal. Despite more pronounced strain peaks for the DFOS subsequently bonded to the surface, the area under the strain curve remains approximately the same, cf. Figure 11.

In summary, it can be stated that with the anchor adhesive used, a stiff bond between the specimen and the DFOS could be achieved even with surface installation, and thus an accurate strain measurement could be carried out. Bonding the stiff ORM-DFOS in a groove with a rough surface texture even had a negative effect on the quality of the strain curve. For strain measurements in the laboratory or short-term measurements on the construction site, it therefore seems appropriate to dispense with the milling of a groove. Due to a lack of experience regarding the durability and weather resistance of the adhesive joint, installation in a groove is nevertheless recommended for long-term measurements. In order to guarantee complete integration of the DFOS into the adhesive matrix, when using high-viscosity adhesives, it is recommended to first fill some adhesive into the groove, then press the DFOS into the adhesive and finally to completely fill the groove with adhesive and smooth it with a spatula. It must be ensured that the DFOS is pressed evenly into the adhesive over the entire length so that a homogeneous bond can be guaranteed.

4.4 | Verification of the crack width calculation

Finally, the potential of the different DFOS types with respect to crack width calculation will be evaluated. The crack widths measured at the surface by using DIC are considered to be the reference value and the measurement deviation Δw_{cr} is therefore defined as:

$$\Delta w_{cr} = w_{cr,DFOS} - w_{cr,DIC} \tag{7}$$

where $w_{cr,DFOS}$ is the crack width calculated by integrating the strain profile of DFOS measurements and $w_{cr,DIC}$ is the reference crack width from DIC. As mentioned before, four relevant cracks appeared on beam 1 in the measuring field of 60 cm. For the second beam, five cracks with crack widths up to 0.33 mm were recorded, giving a total of nine cracks for comparison between DIC and DFOS measurements. A limit value of ±50 μm (= ±0.05 mm) was set as the maximum acceptable deviation for field applications.

In Figure 11, the DFOS are sorted according to the stiffness of the strain transfer in ascending order. The V9 and the NYL-buffered DFOS are advantageous in terms of robustness, but the multilayer structure results in a strongly damped strain signal. This makes accurate localization of cracks and the determination of integration boundaries difficult. The resulting error is reflected in the calculated crack widths. For V9, cracks with spacings of less than 10 cm were smeared within a single strain peak in four cases, significantly overestimating crack widths. In contrast, the DFOS with ACR or ORM coating showed a direct strain transfer with only small shear deformations between the measuring object and the optical fiber resulting in high strain values in the crack openings. Cracks can be reliably detected and precisely localized based on the strain profiles. Except for one outlier with the ORM-DFOS, the determined crack widths showed good agreement with DIC. However, as the strain sensitivity of the DFOS increases, so does the risk of fiber breakage. For both DFOS types, one of three DFOS failed or gave unrealistic results. In addition, measurement anomalies can occur, as has been shown, for example, when measuring inside the groove, cf. Figure 10b. The deployed ES had a good balance between sensitivity in strain measurements and sufficient robustness. All cracks were detected by pronounced strain peaks, precisely localized and the calculated crack widths correlated well with the DIC measurement. The mean absolute deviation $|\Delta w_{cr,mean}|$ was ±0.012 mm and thus clearly exceeded the expectations. The maximum deviation for one crack at beam 2 was 0.045 mm, which means that all values were within the limit of 0.05 mm.

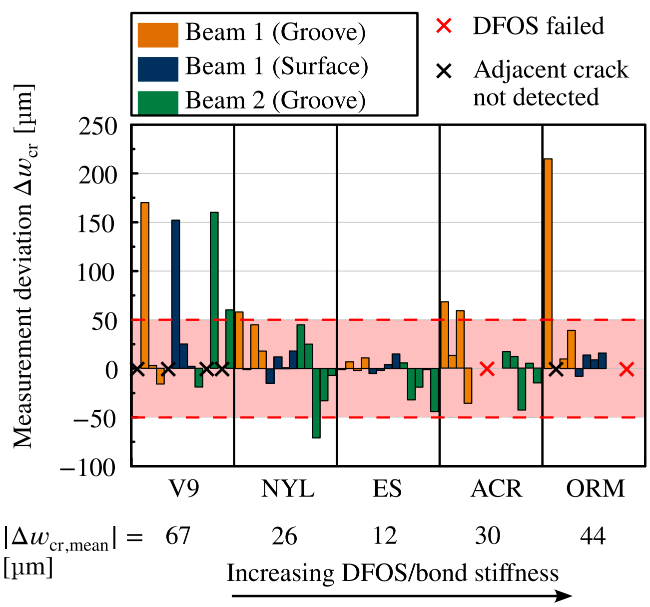

FIGURE 11 Measurement deviations between distributed fiber optic sensors (DFOS) and digital image correlation (DIC) for the analyzed DFOS types.

5 | CONCLUSIONS

For a reliable SHM of existing structures using the technology of fiber optic sensing, the DFOS type and the installation technique must match the specific measurement task. Before large-scale measurements on real structures are carried out, it is advisable to check the suitability of the chosen DFOS type and the application method in preliminary tests.

In this experimental study, five different DFOS types were subsequently bonded to two 4 m long RC beams loaded in a 4-point bending test. To investigate the influence of the DFOS type on the strain transfer mechanisms, both filigree and robust DFOS were used. The DFOS were either installed in a groove or glued directly to the concrete surface. Based on DIC measurements, the suitability of the different DFOS types and application techniques was evaluated for crack monitoring.

Despite the subsequent DFOS installation, the onset of cracking could be indicated at a very early stage. Even fine cracks with crack widths of less than 0.01 mm, which are not visible to the human eye, could be reliably detected via strain peaks. The tested robust DFOS suitable for construction sites showed clear differences in the measured strain profiles. While the monolithic ES was able to reliably capture even closely spaced cracks by single strain peaks, the strain curves measured with the multi-layered sensing cable were strongly attenuated. In SLS, the strain peaks of the ES were about three times higher than those of the V9 (cf. Figure 9). Especially for existing structures, where the cracks have already formed and further changes in the crack openings are small, a stiff strain transfer between the optical fiber and the host material is essential.

These damped strain curves, probably caused by slippage between the individual layers, may lead to misinterpretations. If two cracks are smeared within one strain peak, crack widths are considerably overestimated. For the ES, the calculated crack widths showed an almost perfect agreement with DIC. The maximum measurement deviation for one crack width was 0.045 mm and thus within the limits of $\pm$0.05 mm, which were set as a minimum requirement for practical use. It was demonstrated that crack widths can be determined with high accuracy without the need for analytical models (e.g., shear lag theory[69]).

For laboratory applications, filigree DFOS with an ACR or ORM coating convince with a stiff strain transfer and can be a suitable alternative to the ES. However, in the case of larger crack widths (>0.3 mm), there is an increased risk of measuring sections with implausible strain values or, in the worst case, even fiber breakage.

To achieve a proper bond between the specimens and the DFOS, installation in a groove is not mandatory. With the two-component injection mortar used, even more pronounced strain peaks were observed for the DFOS bonded to the smooth concrete surface. Bonding the DFOS along a groove with high-viscosity adhesives involves the risk not fully embedding the DFOS in the adhesive matrix. For reasons of robustness (e.g., against mechanical impact, fire, etc.) and durability, the installation in a groove is nevertheless recommended to ensure reliable long-term measurements.

The presented study shows the potential of fiber optic measurements for SHM of existing concrete structures. The results provide valuable information for the selection of the DFOS type and its installation. In times of scarce personnel resources, the resource "human" can be used much more efficiently in structural inspection through the use of fiber optic sensing. However, the full potential of DSS can only be revealed when the resulting large amounts of data can be automatically analyzed and evaluated. In this article, theoretical approaches for the crack detection, localization and crack width calculation were presented. Based on these experiments, a PYTHON framework for automated data evaluation was developed and made freely available.[39]

ACKNOWLEDGMENTS

This paper presents some of the results of the research project IDA-KI (Automated assessment of monitoring data for infrastructure constructions using AI and IoT) funded by the Federal Ministry for Digital and Transport, Germany, within the innovation program mFUND (funding reference: 19FS2013A). We would like to thank the funding authority for their financial support as well as the research partners for the productive cooperation within the project. Open Access funding enabled and organized by Projekt DEAL.

CONFLICT OF INTEREST STATEMENT

The authors declare there are no conflicts of interest.

DATA AVAILABILITY STATEMENT

The data that support the findings of this study are available from the corresponding author upon reasonable request.

ORCID

Max Herbers https://orcid.org/0000-0002-2187-1652
Bertram Richter https://orcid.org/0000-0002-3833-8424
Daniel Gebauer https://orcid.org/0000-0002-7298-2395
Martin Classen https://orcid.org/0000-0002-7763-8438
Steffen Marx https://orcid.org/0000-0001-8735-1345

REFERENCES

1. Bundesanstalt für Straßenwesen. Brückenstatistik https://www.bast.de/DE/Statistik/Bruecken/Brueckenstatistik.html. 2021; Accessed 6 Dec 2022.
2. Grabe M, Ullerich C, Wenner M, Herbrand M. smart- Bridge Hamburg – prototypische Pilotierung eines digitalen Zwillings. Bautechnik. 2020;97(2):118–25. https://doi.org/10.1002/bate.201900108
3. Smarsly K, Dragos K, Kölzer T. Sensorintegrierte Digitale Zwillinge für das automatisierte Monitoring von Infrastrukturbauwerken. Bautechnik. 2022;99(6):471–6. https://doi.org/10.1002/bate.202200031
4. Bado MF, Tonelli D, Poli F, Zonta D, Casas JR. Digital twin for civil engineering systems: an exploratory review for distributed sensing updating. Sensors. 2022;22(9):3168. https://doi.org/10.3390/s22093168
5. Farrar CR, Worden K. An introduction to structural health monitoring. Philos Transact A Math Phys Eng Sci. 1851; 2007(365):303–15. https://doi.org/10.1098/rsta.2006.1928
6. Smarsly K, Law KH. Decentralized fault detection and isolation in wireless structural health monitoring systems using analytical redundancy. Adv Eng Software. 2014;73:1–10. https://doi.org/10.1016/j.advengsoft.2014.02.005
7. Herbers M, Wenner M, Marx S. A 576 m long creep and shrinkage specimen—long-term deformation of a semi-integral concrete bridge with a massive solid cross-section. Structural Concrete. 2022. https://doi.org/10.1002/suco.202200599
8. Herbrand M, Lazoglu A, Ullerich C, Marx S, Zehetmaier G. Aggregation von Zustandsindikatoren aus Inspektionsund Monitoringdaten im Brückenbau. Bautechnik. 2022;99(2):95–103. https://doi.org/10.1002/bate.202100095

9. Wedel F, Marx S. Prognose von Messdaten beim Bauwerksmonitoring mithilfe von machine learning. Bautechnik. 2020; 97(12):836–45. https://doi.org/10.1002/bate.202000073
10. Farrar CR. Structural health monitoring: a machine learning perspective. Chichester, West Sussex, U.K and Hoboken, N.J: Wiley; 2013.
11. Al-Zuriqat T, Chillón Geck C, Dragos K, Smarsly K. Adaptive fault diagnosis for simultaneous sensor faults in structural health monitoring systems. Inf Dent. 2023;8(3):39. https://doi.org/10.3390/infrastructures8030039
12. Herrmann R, Stockmann M, Marx S. Untersuchungsstrategie zur Bewertung der Langzeitstabilität von Dehnungsmessstreifen. Bautechnik. 2015;92(7):451–60. https://doi.org/10.1002/bate.201500018
13. Schnellenbach-Held M, Peeters M, Miedzinski G. Intelligente Brücke—Schädigungsrelevante Einwirkungen und Schädigungspotenziale von Brückenbauwerken aus Beton. Tech. Rep. B 110, Bundesanstalt für Straßenwesen; Bergisch Gladbach 2015.
14. Erdenebat D, Waldmann D. Application of the DAD method for damage localisation on an existing bridge structure using close-range UAV photogrammetry. Eng Struct. 2020;218: 110727. https://doi.org/10.1016/j.engstruct.2020.110727
15. Flotzinger J, Braml T. Automatisierte Klassifizierung von Schäden an Massivbrücken mittels Neuronaler Netze. Beton-Und Stahlbetonbau. 2022;117(10):786–94. https://doi.org/10.1002/best.202200068
16. Ungermann J, Schmidt P, Classen M, Hegger J. Eccentric punching tests on column bases—new insights into the inner concrete strain development. Eng Struct. 2022;262:114273. https://doi.org/10.1016/j.engstruct.2022.114273
17. Becks H, Bielak J, Camps B, Hegger J. Application of fiber optic measurement in textile–reinforced concrete testing. Structural Concrete. 2022;23(4):2600–14. https://doi.org/10.1002/suco.202100252
18. Becks H, Baktheer A, Marx S, Classen M, Hegger J, Chudoba R. Monitoring concept for the propagation of compressive fatigue in externally prestressed concrete beams using digital image correlation and fiber optic sensors. Fatigue Fract Eng Mater Struct. 2023;46(2):514–26. https://doi.org/10.1111/ffe.13881
19. Barrias A, Casas JR, Villalba S. A review of distributed optical fiber sensors for civil engineering applications. Sensors. 2016; 16(5):748. https://doi.org/10.3390/s16050748
20. Bado MF, Casas JR. A review of recent distributed optical fiber sensors applications for civil engineering structural health monitoring. Sensors (Basel, Switzerland). 2021;21(5):1818. https://doi.org/10.3390/s21051818
21. Speck K, Vogdt F, Curbach M, Petryna Y, Marx S. Dehnungsmessung bei mehraxialen Druckversuchen an Beton mittels faseroptischer Sensoren. Betonund Stahlbetonbau. 2021;116(3): 212–21. https://doi.org/10.1002/best.202000095
22. Koschemann M, Curbach M, Marx S. Investigation of local bond behavior using distributed optical fiber sensing. In: Hofmann J, Plizzari G, editors. Proceedings of 5th int. conference bond in concrete. Stuttgart: Universität Stuttgart; 2022. p. 133–45.
23. Zdanowicz K, Gebauer D, Koschemann M, Speck K, Steinbock O, Beckmann B, et al. Distributed fiber optic sensors for measuring strains of concrete, steel, and textile reinforcement: possible fields of application. Structural Concrete. 2022;23:3367–82. https://doi.org/10.1002/suco.202100689
24. Gómez J, Casas JR, Villalba S. Structural health monitoring with distributed optical fiber sensors of tunnel lining affected by nearby construction activity. Autom Constr. 2020;117:103261. https://doi.org/10.1016/j.autcon.2020.103261
25. Grunicke UH, Lienhart W, Vorwagner A. Long–term monitoring of visually not inspectable tunnel linings using fibre optic sensing. Geomech Tunn. 2021;14(1):19–32. https://doi.org/10.1002/geot.202000051
26. Monsberger CM, Lienhart W. Distributed fiber optic shape sensing along shotcrete tunnel linings: methodology, field applications, and monitoring results. J. Civ Struct Health Monit. 2021;11(2):337–50. https://doi.org/10.1007/s13349-020-00455-8
27. Barrias A, Rodriguez G, Casas JR, Villalba S. Application of distributed optical fiber sensors for the health monitoring of two real structures in Barcelona. Struct. Infrastruct. Eng. 2018;14(7):967–85. https://doi.org/10.1080/15732479.2018.1438479
28. Novák B, Stein F, Reinhard J, Dudonu A. Einsatz kontinuierlicher faseroptischer Sensoren zum Monitoring von Bestandsbrücken. Beton- Und Stahlbetonbau. 2021;116(10):718–26. https://doi.org/10.1002/best.202100070
29. Bednarski Ł, Sieńko R, Howiacki T, Zuziak K. The smart nervous system for cracked concrete structures: theory, design, research, and field proof of monolithic DFOS-based sensors. Sensors (Basel, Switzerland). 2022;22(22):8713. https://doi.org/10.3390/s22228713
30. Howiacki T, Sieńko R, Bednarski Ł, Zuziak K. Crack shape coefficient: comparison between different DFOS tools embedded for crack monitoring in concrete. Sensors. 2023;23(2):566. https://doi.org/10.3390/s23020566
31. Fischer O, Thoma S, Crepaz S. Distributed fiber optic sensing for crack detection in concrete structures. Civ Eng Des. 2019;1(3–4):97–105. https://doi.org/10.1002/cend.201900008
32. Berrocal C, Fernandez I, Rempling R. Crack monitoring in reinforced concrete beams by distributed optical fiber sensors. Struct Infrastruct Eng. 2020;17(1):124–39. https://doi.org/10.1080/15732479.2020.1731558
33. Brault A, Hoult N. Monitoring reinforced concrete serviceability performance using fiber optic sensors. ACI Structur J. 2019; 116(1):57–70. https://doi.org/10.14359/51710870
34. Wedel F, Marx S. Application of machine learning methods on real bridge monitoring data. Eng Struct. 2022;250:113365. https://doi.org/10.1016/j.engstruct.2021.113365
35. Bremer K, Alwis LSM, Zheng Y, Weigand F, Kuhne M, Helbig R, et al. Durability of functionalized carbon structures with optical fiber sensors in a highly alkaline concrete environment. Appl Sci. 2019;9(12):2476. https://doi.org/10.3390/app9122476
36. Habel W. Faseroptische Sensoren für hochaufgelöste Verformungsmessungen in der Zementsteinmatrix: Forschungsbericht 246. Bremerhaven, Germany: Wirtschaftsverlag NW; 2003.
37. Alj I, Quiertant M, Khadour A, Grando Q, Benzarti K. Environmental durability of an optical fiber cable intended for

distributed strain measurements in concrete structures. Sensors (Basel, Switzerland). 2021;22(1). https://doi.org/10.3390/s22010141

38. Tan X, Bao Y. Measuring crack width using a distributed fiber optic sensor based on optical frequency domain reflectometry. Measurement. 2021;172:108945. https://doi.org/10.1016/j.measurement.2020.108945
39. Richter B, Herbers M, Marx S. Crack monitoring on concrete structures with distributed fiber optic sensors – towards automated data evaluation and assessment. Structural Concrete. 2023; (under review).
40. Bao X, Chen L. Recent progress in distributed fiber optic sensors. Sensors. 2012;12(7):8601–39. https://doi.org/10.3390/s120708601
41. Clauß F, Ahrens MA, Mark P. Thermo–mechanical experiments on reinforced concrete beams: assessing thermal, mechanical, and mixed impacts on fiber optic measurements. Structural Concrete. 2022;23(6):3521–37. https://doi.org/10.1002/suco.202100890
42. Ouyang J, Chen X, Huangfu Z, Lu C, Huang D, Li Y. Application of distributed temperature sensing for cracking control of mass concrete. Construct Build Mater. 2019;197:778–91. https://doi.org/10.1016/j.conbuildmat.2018.11.221
43. Wang W, Chang J, Lv G, Wang Z, Liu Z, Luo S, et al. Wavelength dispersion analysis on fiber-optic Raman distributed temperature sensor system. Photonic Sens. 2013;3(3):256–61. https://doi.org/10.1007/s13320-013-0102-y
44. Janani R, Majumder D, Scrimshire A, Stone A, Wakelin E, Jones AH, et al. From acrylates to silicones: a review of common optical fibre coatings used for normal to harsh environments. Prog Org Coat. 2023;180:107557. https://doi.org/10.1016/j.porgcoat.2023.107557
45. Mata-Falcón J, Haefliger S, Lee M, Galkovski T, Gehri N. Combined application of distributed fibre optical and digital image correlation measurements to structural concrete experiments. Eng Struct. 2020;225:111309. https://doi.org/10.1016/j.engstruct.2020.111309
46. Chapeleau X, Bassil A. A general solution to determine strain profile in the Core of distributed fiber optic sensors under any arbitrary strain fields. Sensors. 2021;21(16). https://doi.org/10.3390/s21165423
47. Speck K, Vogdt F, Curbach M, Petryna Y. Faseroptische Sensoren zur kontinuierlichen Dehnungsmessung im Beton. Beton- Und Stahlbetonbau. 2019;114(3):160–7. https://doi.org/10.1002/best.201800105
48. Weisbrich M, Holschemacher K. Comparison between different fiber coatings and adhesives on steel surfaces for distributed optical strain measurements based on Rayleigh backscattering. J Sens Sens Systems. 2018;7(2):601–8. https://doi.org/10.5194/jsss-7-601-2018
49. Weisbrich M, Holschemacher K, Bier T. Comparison of different fiber coatings for distributed strain measurement in cementitious matrices. J Sens Sens Syst. 2020;9(2):189–97. https://doi.org/10.5194/jsss-9-189-2020
50. Zhang S, Liu H, Coulibaly AAS, DeJong M. Fiber optic sensing of concrete cracking and rebar deformation using several types of cable. Struct Control Health Monit. 2020;28(2). https://doi.org/10.1002/stc.2664
51. Henault JM, Quiertant M, Delepine-Lesoille S, Salin J, Moreau G, Taillade F, et al. Quantitative strain measurement and crack detection in RC structures using a truly distributed fiber optic sensing system. Construct Build Mater. 2012;37:916–23. https://doi.org/10.1016/j.conbuildmat.2012.05.029
52. Bado MF, Casas JR, Barrias A. Performance of Rayleigh-based distributed optical fiber sensors bonded to reinforcing bars in bending. Sensors. 2018;18(9):3125. https://doi.org/10.3390/s18093125
53. Bado MF, Casas JR, Dey A, Berrocal CG. Distributed optical fiber sensing bonding techniques performance for embedment inside reinforced concrete structures. Sensors. 2020;20(20):5788. https://doi.org/10.3390/s20205788
54. Brault A, Hoult N. Distributed reinforcement strains: measurement and application. ACI Structur J. 2019;116(4):115–27. https://doi.org/10.14359/51714483
55. Bastianini F, Di Sante R, Falcetelli F, Marini D, Bolognini G. Optical fiber sensing cables for Brillouin-based distributed measurements. Sensors. 2019;19(23):5172. https://doi.org/10.3390/s19235172
56. Vorwagner A, Kwapisz M, Lienhart W, Winkler M, Monsberger C, Prammer D. Verteilte Rissbreitenmessung im Betonbau mittels faseroptischer Sensorik – Neue Anwendung von verteilten faseroptischen Messsystemen. Beton- Und Stahlbetonbau. 2021;116(10):727–40. https://doi.org/10.1002/best.202100060
57. Clauß F, Ahrens MA, Mark P. A comparative evaluation of strain measurement techniques in reinforced concrete structures–a discussion of assembly, application, and accuracy. Structural Concrete. 2021;22(5):2992–3007. https://doi.org/10.1002/suco.202000706
58. Her SC, Huang CY. The effects of adhesive and bonding length on the strain transfer of optical fiber sensors. Appl Sci. 2016;6(1):13. https://doi.org/10.3390/app6010013
59. Alj I, Quiertant M, Khadour A, Grando Q, Terrade B, Renaud JC, et al. Experimental and numerical investigation on the strain response of distributed optical fiber sensors bonded to concrete: Influence of the adhesive stiffness on crack monitoring performance. Sensors (Basel, Switzerland). 2020;20(18). https://doi.org/10.3390/s20185144
60. Fernandez I, Berrocal CG, Rempling R. Long-term performance of distributed optical fiber sensors embedded in reinforced concrete beams under sustained deflection and cyclic loading. Sensors. 2021;21(19):6338. https://doi.org/10.3390/s21196338
61. Rodríguez G, Casas JR, Villaba S. Cracking assessment in concrete structures by distributed optical fiber. Smart Mater Structur. 2015;24(3):035005. https://doi.org/10.1088/0964-1726/24/3/035005
62. Sieńko R, Zych M, Bednarski Ł, Howiacki T. Strain and crack analysis within concrete members using distributed fibre optic sensors. Structur Health Monitor. 2018;18(5–6):1510–26. https://doi.org/10.1177/1475921718804466
63. Regier RR. Application of fibre optics on reinforced concrete structures to develop a structural health monitoring technique. Master's thesis. Queen's University. Canada. 2013.
64. Regier R, Hoult NA. Concrete deterioration detection using distributed sensors. Proc Inst Civ Eng: Struct Build. 2015;168(2):118–26. https://doi.org/10.1680/stbu.13.00070
65. Villalba S, Casas JR. Application of optical fiber distributed sensing to health monitoring of concrete structures. Mech Syst Signal Process. 2013;39(1–2):441–51. https://doi.org/10.1016/j.ymssp.2012.01.027

66. Barrias A, Casas JR, Villalba S. Distributed optical fibre sensors in concrete structures: performance of bonding adhesives and influence of spatial resolution. Struct Control Health Monit. 2018;26(3):e2310. https://doi.org/10.1002/stc.2310
67. Rodriguez G, Casas JR, Villalba S. Shear crack width assessment in concrete structures by 2D distributed optical fiber. Eng Struct. 2019;195:508–23. https://doi.org/10.1016/j.engstruct.2019.05.079
68. Her SC, Huang CY. Effect of coating on the strain transfer of optical fiber sensors. Sensors. 2011;11(7):6926–41. https://doi.org/10.3390/s110706926
69. Feng X, Zhou J, Sun C, Zhang X, Ansari F. Theoretical and experimental investigations into crack detection with BOTDR-distributed fiber optic sensors. J Eng Mech. 2013;139:1797–807. https://doi.org/10.1061/(ASCE)EM.1943-7889.0000622
70. Bassil A, Chapeleau X, Leduc D, Abraham O. Concrete crack monitoring using a novel strain transfer model for distributed fiber optics sensors. Sensors (Basel, Switzerland). 2020;20(8):2220. https://doi.org/10.3390/s20082220
71. International Federation for Structural Concrete. Fib model code for concrete structures 2010. fib CEBFIPBerlin: Ernst & Sohn; 2013.
72. Deutsches Institut für Normung e.V. DINNormenausschuss Bauwesen. *Eurocode 2: Bemessung und Konstruktion von Stahlbeton- und Spannbetontragwerken—Teil 1–1: Allgemeine Bemessungsregeln und Regeln für den Hochbau; Deutsche Fassung EN 1992–1-1:2004 + AC:2010*. Berlin: Beuth Verlag GmbH. 1 Jan 2011.
73. CEN. EN 12390–3:2019: Testing hardened concrete. Part 3: Compressive strength of test specimens; 2019.
74. CEN. EN 12390–13:2021: Testing hardened concrete. Part 13, Determination of secant modulus of elasticity in compression; 2021.
75. CEN. EN 12390–6:2009: Testing hardened concrete. Part 6: Tensile splitting strength of test specimens; 2009.
76. CEN. EN 12390–5:2019: Testing hardened concrete. Part 5: Flexural strength of test specimens; 2019.
77. Optical Distributed Sensor Interrogator Model ODiSI 6: User's Guide ODiSI 6 Software. https://lunainc.com/sites/default/files/assets/files/resource-library/ODiSI%206100%20User%20Guide.pdf; 2020. Accessed 25 Oct 2022

AUTHOR BIOGRAPHIES

Max Herbers, Technische Universität Dresden, Institute of Concrete Structures, 01062 Dresden, Germany. Email: max.herbers@tu-dresden.de

Bertram Richter, Technische Universität Dresden, Institute of Concrete Structures, 01062 Dresden, Germany.

Daniel Gebauer, Technische Universität Dresden, Institute of Concrete Structures, 01062 Dresden, Germany.

Martin Classen, RWTH Aachen, Institute of Structural Concrete, 52074 Aachen, Germany.

Steffen Marx, Technische Universität Dresden, Institute of Concrete Structures, 01062 Dresden, Germany.

How to cite this article: Herbers M, Richter B, Gebauer D, Classen M, Marx S. Crack monitoring on concrete structures: Comparison of various distributed fiber optic sensors with digital image correlation method. Structural Concrete. 2023. https://doi.org/10.1002/suco.202300062